Broadband High-Efficiency Power Amplifier With Quasi-Elliptic Low-Pass Response

HANG CHEN[1], **JIN-XU XU**[1,2], **ZHI-HUA KONG**[1], **WEN-HUA CHEN**[3], **(Senior Member, IEEE)**, **AND XIU YIN ZHANG**[1], **(Senior Member, IEEE)**

[1]School of Electronic and Information Engineering, South China University of Technology, Guangzhou 510641, China
[2]School of Electrical and Data Engineering, University of Technology Sydney, Ultimo, NSW 2007, Australia
[3]School of Electronic Engineering, Tsinghua University, Beijing 100084, China

Corresponding author: Jin-Xu Xu (xjinxu@126.com)

ABSTRACT This paper presents a broadband high-efficiency harmonic-tuned power amplifier (PA) with quasi-elliptic low-pass responses. A combination of continuous Class-F^{-1} and extended continuous Class-F PA modes is employed to significantly expand the design space. A quasi-elliptic low-pass matching network is proposed, which can realize a broadband impedance matching in the predefined optimal impedance region desired by the combination of PA modes. Furthermore, two transmission zeros are generated near the passband, exhibiting high skirt selectivity and providing rapid impedance transition from the passband to the stopband. A wide stopband covering up to the third harmonic is achieved which shows good harmonic suppression. Design procedures of the proposed broadband PA are presented. To verify the proposed methodology, the broadband PA is fabricated and measured. The implemented PA achieves a bandwidth of 145.2% from 0.5 to 3.15 GHz. Over this frequency range, the drain efficiency is measured as 58-74.9% with the output power of greater than 39.03 dBm and a large signal gain ranging from 8.43 to 15.67 dB. A wide stopband is realized from 3.4 to 10 GHz, showing excellent quasi-elliptic low-pass responses. The measured adjacent leakage ratios (ACLRs) using a 20-MHz LTE signal with digital pre-distortion are below -45.06 dBc.

INDEX TERMS Broadband power amplifier, filter-integrated power amplifier, harmonic suppression, high efficiency, quasi-elliptic low-pass matching network.

I. INTRODUCTION

The power amplifier (PA) is one of the most important devices in radio frequency (RF) transceivers. In recent years, co-designs of filters and PAs have drawn much attention. For example, in [1]–[4], bandpass filters (BPFs) are utilized as the output matching networks (OMNs) of PAs, which can integrate bandpass responses to the PAs and also improve the overall efficiency of the PA and filter. In [5]–[7], the notched-band ultra-wideband BPF, low-pass filter, and compact microstrip resonant cell are employed to optimize the harmonics in Class-F PAs to realize high efficiency. However, these filter-integrated PAs [1]–[7] are designed for narrowband applications.

With the rapid development of wireless technologies, an ever-increasing number of frequency bands are utilized

The associate editor coordinating the review of this manuscript and approving it for publication was Feng Lin.

to meet the requirement of Gb/s peak data transmission ratios and network capacity in emerging mobile systems. Thus, PAs are often required to operate over a wide bandwidth with reduced power consumption. Subsequently, some filter-integrated PAs are also designed for broadband applications. In [8], a broadband continuous inverse Class-F (CCF^{-1}) is presented using a modified elliptic low-pass filtering matching network. In [9], a ring-resonator filter is used to achieve broadband impedance matching, where transmission zeros (TZs) can be introduced to suppress the second harmonic. The real frequency technique with finite transmission zeros is also extensively studied to realize a broadband CCF PA [10]. Using in-band continuous Class-F (CCF) and CCF^{-1} mode transferring, a PA can be designed with wider bandwidth based on a low-pass impedance transformer [11]. Apart from the filter-based CCF and CCF^{-1} PAs in [8]–[11], the extended CCF or CCF^{-1} PA modes can be used for further operational bandwidth expansion [12]–[14].

In this paper, a novel quasi-elliptic low-pass output matching network (LP OMN) is proposed to design the high-efficiency broadband PAs using the combined modes of the CCF^{-1} and extended CCF PA modes. The proposed filter-integrated broadband PA shows excellent quasi-elliptic low-pass responses with a more than two-octave operation bandwidth of 145.2%. A swift impedance transition from the operation passband to the stopband and a harmonic suppression up to the third harmonic are also realized. The rest of this paper is organized as follows. Section II presents the analysis of the proposed broadband PA using LP OMN based on the combination of CCF^{-1} and extended CCF PA modes. Then, design procedures and waveform engineering are given in Section III. For validation, simulated and measured results are shown in Section IV. Finally, a conclusion is given in Section V.

II. DESIGN METHODOLOGY

In this section, the design methodology of the proposed broadband PA with quasi-elliptic low-pass responses is presented. Firstly, theoretical analyses of the operation CCF^{-1} and extended CCF PA modes are given, which indicate that the combined PA modes and allowing resistive second harmonic impedance can relax the broadband PA design space. Then, the design method of the proposed LP OMN is detailed for achieving wide operation bandwidth and high efficiency.

A. CCF^{-1} AND EXTENDED CCF PA MODES

For a CCF^{-1} PA mode, theoretical design space at current generate (I-gen) plane can be expressed in an admittance format as [12]

$$Y_1 = \sqrt{2}\,(0.43 + j * 0.37\zeta)\,G_{opt} \qquad (1a)$$

$$Y_2 = -j * 0.98 * \zeta * G_{opt} \qquad (1b)$$

$$Y_3 = \infty \qquad (1c)$$

where Y_n (n = 1, 2, 3) refers to the n-th harmonic admittance. While the theoretical design space at I-gen plane of the extended CCF PA mode can be expressed in the impedance format as [13]

$$Z_1 = \left(\frac{2}{\sqrt{3}} - \delta\right) R_{opt} + j\left(1 - \frac{7}{12\sqrt{3}}\right) R_{opt}\gamma \qquad (2a)$$

$$Z_2 = \frac{3\pi}{8}\left(\frac{5}{3\sqrt{3}}R_{opt}\delta - j\left(\frac{7}{3\sqrt{3}} - \delta\right)R_{opt}\gamma\right) \qquad (2b)$$

$$Z_3 = \infty \qquad (2c)$$

where Z_n refers to the n-th harmonic impedance, γ, δ, ζ are empiric parameters that define the design space, R_{opt} is the optimum impedance of standard Class-B PA mode and $G_{opt} = 1/R_{opt}$. To guarantee a positive voltage of the extended CCF PA mode and a nonzero crossing current waveform of the CCF^{-1} PA mode, the value of γ and ζ should vary from −1 to 1 [12], [13]. Simultaneously, in order to ensure that the second-harmonic impedances are inside the Smith chart,
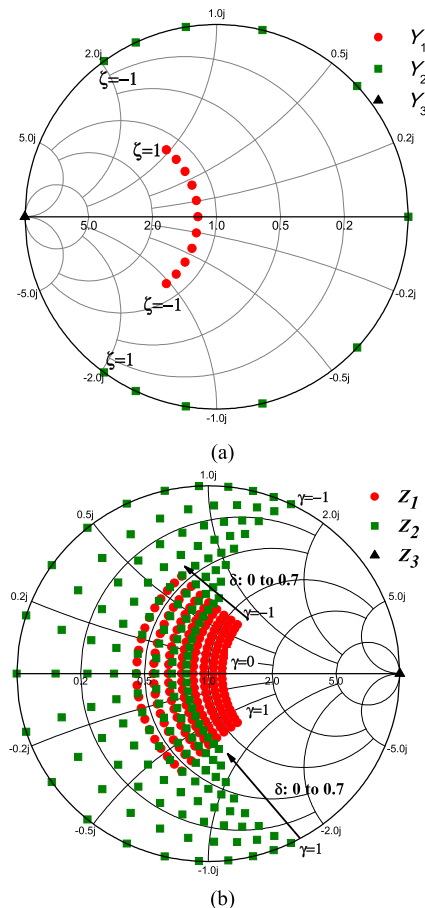

FIGURE 1. Calculated first three loads. (a). CCF^{-1} mode in the admittance chart (b). Extended CCF mode in the impedance chart.

the value of δ should be confined between 0 and 1 according to (2b).

According to (1) and (2), the design spaces of CCF^{-1} and extended CCF PA modes are presented on Smith charts, as shown in Figs. 1(a) and (b), respectively. It is noted that the overlap between the fundamental and second harmonic impedances is allowed in the extended mode, which means that wider design spaces of the extended CCF PA modes can be obtained. Moreover, a combination of these two continuous PA modes can further expand the design space.

Based on the above-mentioned analysis, a broadband PA is proposed by the combination of CCF^{-1} and extended CCF PA modes. The PA configuration mainly consists of an input matching network (IMN), a transistor and an OMN. For the IMN, it can be designed based on step-impedance transmission lines [15] to realize the broadband matching. To achieve optimal performance over a wide bandwidth, the key point is to design the OMN to fit the derived design spaces in Fig. 1. To meet the requirement, a novel quasi-elliptic LP OMN is proposed as shown in Fig. 2, which consists of the transmission lines TL0-TL4 in series and TB1, TS1, TS2 in parallel. It is utilized to realize wideband harmonic suppression and impedance matching, as analyzed below.
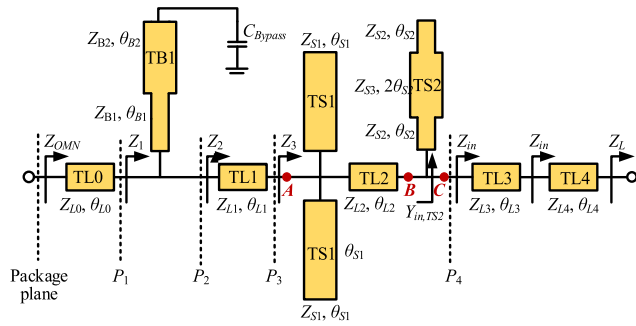
FIGURE 2. Schematic of the quasi-elliptic LPF OMN.

B. DESIGN OF HARMONIC TUNING NETWORK

The harmonic tuning network consists of the elements from plane P3 to P4 and TB1 in Fig. 2. Theoretical analyses of the design parameters are addressed as follows.

To start with, the operation passband from 0.5 GHz to 3.15 GHz is divided into two parts, including the lower operation band from f_{L1} to f_{L2} (0.5-1.6 GHz) working at the extended CCF PA mode allowing the resistive second harmonic impedance and the higher operation band from f_{H1} to f_{H2} (1.7-3.15 GHz) working at CCF^{-1} PA mode.

The best solution for harmonic impedances is usually located at the edge of the Smith Chart. Thus, for the CCF^{-1} PA mode, wideband harmonics suppression introduced by the OMN from $2f_{H1}$ to $3f_{H2}$ (3.4-9.45 GHz) is necessary. Here, we firstly analyze the parallel-connected TS2 in Fig. 2, which is used to generate two TZs with a relatively large frequency interval to suppress the harmonics. By solving the input admittance of TS2 as $Y_{in,TS2} = 0$ and $Y_{in,TS2} = \infty$, the circuit from Nodes *B* to *C* in Fig. 2 can generate a reflection zero at f_{rz} and TZs at f_{tz}, respectively. The electrical length θ_{S2} corresponding to f_{rz} and f_{tz} can be obtained as [16]:

$$\theta_{S2}^{@f_{rz}} = \tan^{-1}\sqrt{R_Z} \tag{3}$$

$$\theta_{S2}^{@f_{tz}} = \tan^{-1}\sqrt{\frac{a \pm \sqrt{a^2 - R_Z^2}}{R_Z}} \tag{4}$$

where $a = 1 + R_Z + R_Z^2$, and $R_Z = Z_{S2}/Z_{S3}$ is the characteristic impedance ratio of different transmission line sections in TS2.

From (3) and (4), it can be known that the frequencies of TZs are mainly determined by the value of R_Z and can be normalized by the frequency of the reflection zero as:

$$\frac{f_{tz}}{f_{rz}} = \frac{\theta_{S2}^{@f_{tz}}}{\theta_{S2}^{@f_{rz}}} \tag{5}$$

Accordingly, the normalized frequencies of the first two transmission zeros (f_{tz1} and f_{tz2}) against R_z are illustrated in Fig. 3. As can be seen, when R_z is selected with a smaller value, f_{tz1} and f_{tz2} move to higher frequencies and the interval between them become larger which means the possibility to achieve a wider stopband.
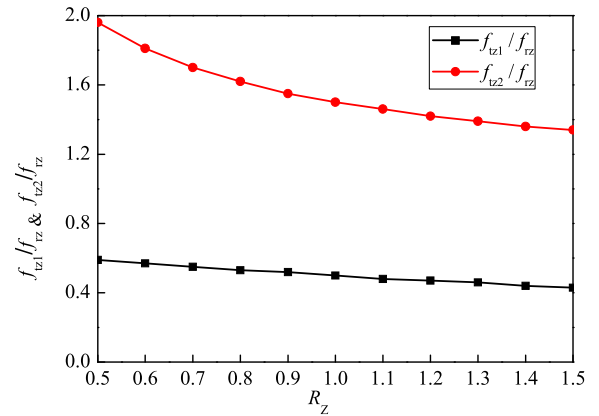

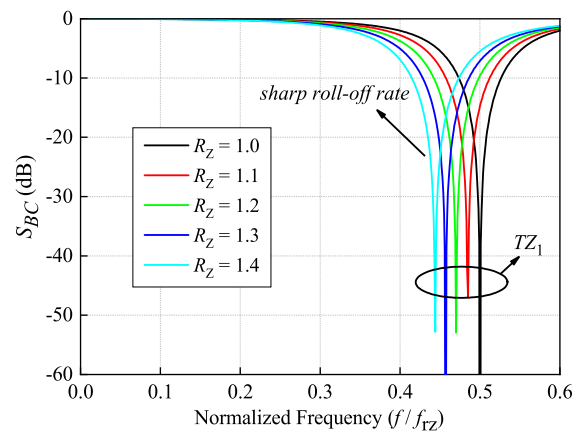**FIGURE 3.** Frequencies of TZs against R_Z ($Z_{S2} = 90\ \Omega$ is fixed).

FIGURE 4. Simulated S_{BC} with different values of R_Z.

To obtain the electric length and characteristic impedance of TS2, we can analyze the parameters of R_Z and Z_{S2}. Based on (3)-(5), the transmission coefficient from Nodes *B* to $C(S_{BC})$ in Fig. 2 under varied values of R_Z can be shown in Fig. 4. As seen, when R_Z increases, a better roll-off rate from the passband to the stopband can be obtained, which is desired by the CCF^{-1} PA mode to have a quick attenuation from the fundamental passband edge f_{H2} (3.15GHz) to the second harmonic $2f_{H1}$ (3.4 GHz). However, it can be found in Fig. 3 that a larger value of R_Z leads to a small interval between f_{tz1} and f_{tz2}, which means a narrower stopband. Thus, there is a trade-off between the roll-off rate and stopband bandwidth.

Based on Figs. 3 and 4, R_z is determined as 1.2 to obtain a sharper roll-off rate and a relatively wide stopband. After obtaining R_z, θ_{S2} corresponding to f_{rz} and f_{tz} can be solved by using (3) and (4), respectively. To determine the value of Z_{S2}, the S_{BC} with different values of Z_{S2} is studied in Fig. 5. It concludes that a lager Z_{S2} contributes to a sharper roll-off rate. Accordingly, an initial value of Z_{S2} is selected as 100 Ω for the sake of practical printed circuit board (PCB) implementation. The value of Z_{S3} can be obtained by the fact that $R_Z = Z_{S2} / Z_{S3}$. Till now the design parameters of TS2 have been determined.
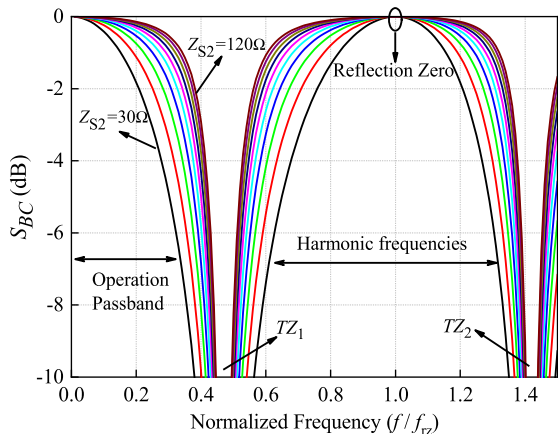
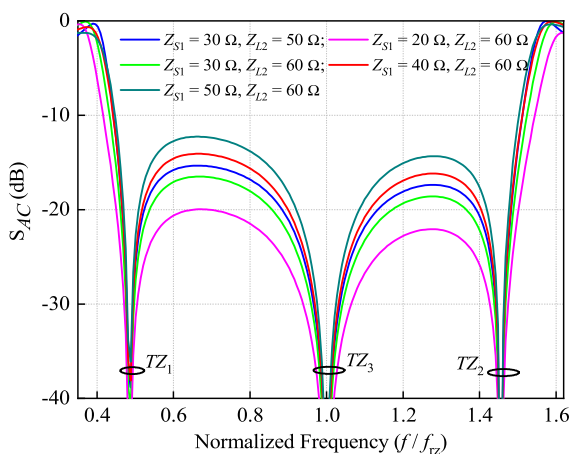**FIGURE 5.** Simulated S_{BC} with different values of Z_{S2}.

FIGURE 6. Simulated S_{AC} with different values of Z_{S1} and Z_{L2}.

As shown in Fig. 5, although two TZs (TZ_1 and TZ_2) are generated with a large frequency interval, the required harmonics suppression from $2f_{H1}$ to $3f_{H2}$ is still not achieved because there is a reflection zero between TZ_1 and TZ_2. To solve this problem, two open-end parallel-connected stubs (TS1) are utilized to generate a TZ (TZ_3) at the frequency of the reflection zero (f_{rz}), and the reason for using two shunt stubs (TS1) here is to reduce the line width. Thus, the electric length of TS1 (θ_{S1}) corresponding to f_{rz} can be easily determined as quarter-wavelength, namely,

$$\theta_{S1}^{@f_{rz}} = 90° \qquad (6)$$

A transmission line TL2 with the electric length of quarter-wavelength is utilized to connect the TS1 and TS2, namely,

$$\theta_{L2}^{@f_{rz}} = 90° \qquad (7)$$

So far, a total of three transmission zeros are generated by the circuit from Nodes *A* to *C* in Fig. 2, which can form a wide stopband, as shown in Fig. 6. It can be seen that the rejection level is influenced by the values of Z_{S1} and Z_{L2}. Based on these simulated results, Z_{S1} is chosen as 30 Ω in view of the limitation of practical PCB implementation and

Z_{L2} is chosen as 60 Ω, which contributes to relatively high harmonic suppression level.

In circuit design, the value of f_{rz} should be determined to meet the desired operation passband frequencies from f_{L1} to f_{H2} (0.5-3.15 GHz) and stopband frequencies from $2f_{H1}$ to $3f_{H2}$ (3.4-9.45 GHz). Thus, the lower end of the stopband (around $0.41f_{rz}$ in Fig. 6) should be larger than f_{H2} (3.15 GHz). In this condition, the initial value of f_{rz} is selected as 7.7 GHz.

As shown in Fig. 6, the frequency of TZ_1 is located at $0.47f_{rz}$(3.62 GHz), which is a bit higher than $2f_{H1}$ (3.4 GHz). In order to further improve the aforementioned roll-off rate from the passband to stopband, which is necessary for the higher operation band working at the CCF^{-1} PA mode, a stepped-impedance transmission line (TB1) with the equivalent electric length of quarter-wavelength ($\lambda_g/4$) at f_{H1} is introduced to generate a TZ (TZ_0) at $2f_{H1}$. In addition, TB1 is also employed to offer wideband bias for the transistor. The design parameters of TB1 can be obtained by using the same analysis method as the above-mentioned analyses of TS2, which is not detailed here for brevity.

After realizing wideband harmonic suppression, transmission lines TL0 and TL1 in Fig. 2 are introduced as tuning lines to ensure the harmonic impedances can fit the derived design space as shown in Fig. 1.

C. FUNDAMENTAL IMPEDANCE MATCHING

For the proposed wideband PA, apart from the wideband harmonic suppression, wideband fundamental impedance matching should also be realized over a bandwidth from f_{L1} to f_{H2} (0.5-3.15 GHz). Thus, transmission lines TL3 and TL4 in Fig. 2 are introduced. The relationship between the impedance Z_{in} at plane P4 in Fig. 2 and load impedance Z_L is expressed as (8), as shown at the bottom of the next page.

In order to obtain the value of the design parameters (Z_{L3}, $\theta_{L3}, Z_{L4}, \theta_{L4}$), the entire bandwidth can be separated into four frequency sections and the lower frequency section should have narrower bandwidth [17]. Moreover, in each frequency section, the optimal fundamental impedance at one frequency point needs to be chosen to achieve the desired performance over the corresponding frequency section. Due to the parameters at the left side of plane P4 have been determined, Z_{in} can be obtained by converting the optimal fundamental impedance at the package plane to P4. Then, four parameters of TL3 and TL4 can be solved by using four equations related to four frequency points.

III. BROADBAND PA DESIGN
A. BROADBAND PA DESIGN PROCEDURE
Based on the proposed LP OMN, a broadband PA is designed using a 10-W GaN HEMT packaged transistor (CGH40010F from CREE). In simulation, the equivalent nonlinear large-signal model in Fig. 7 is used [18]. The circuit is designed on the Rogers RO4003C substrate with a relative dielectric constant 3.38, thickness of 0.813 mm and loss tangent of
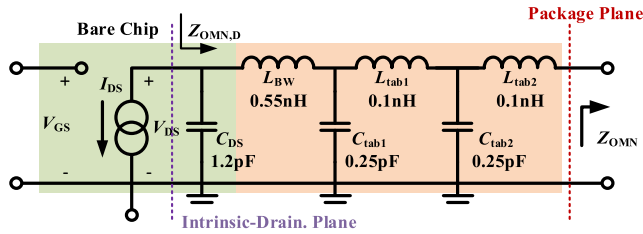
FIGURE 7. Equivalent large-signal circuit model of the transistor CGH40010F.
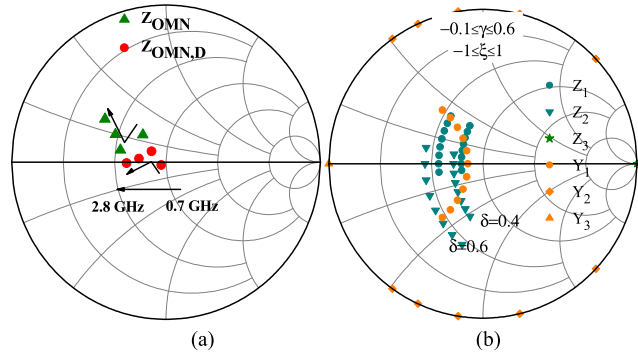

FIGURE 8. (a) Simulated optimal load impedances at 0.7 GHz, 1.2 GHz, 1.9 GHz and 2.8 GHz; (b) Extended impedance ranges of the combined extended CCF and CCF^{-1} modes.
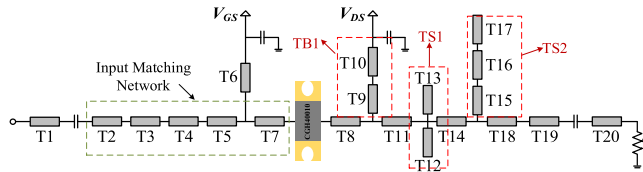

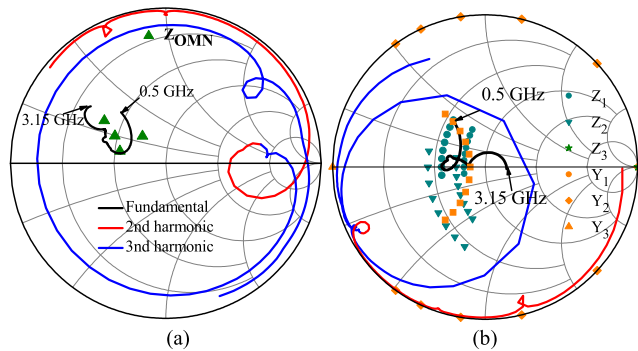
FIGURE 9. Schematic of the proposed broadband PA.

FIGURE 10. Simulated impedances (a) At package plane; (b) At intrinsic-drain plane.

FIGURE 11. Theoretical and simulated voltage and current waveforms at the intrinsic-drain plane (a) At 1 GHz; (b) At 2 GHz. (c) At 3 GHz.

0.0027. The gate and drain bias voltages are chosen as $V_{GS} = -3.1$ V and $V_{DS} = 28$ V, respectively.

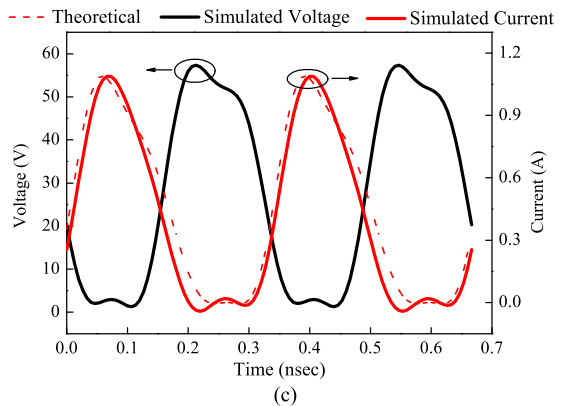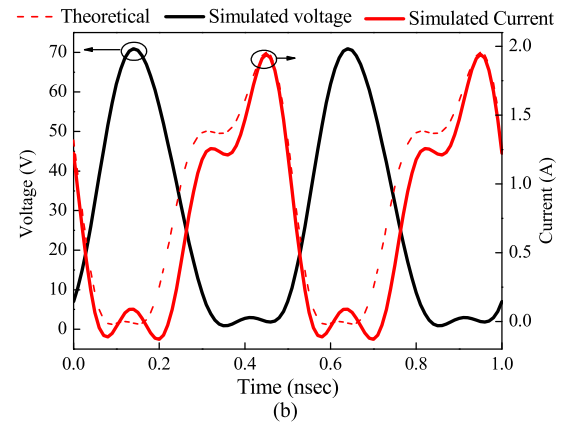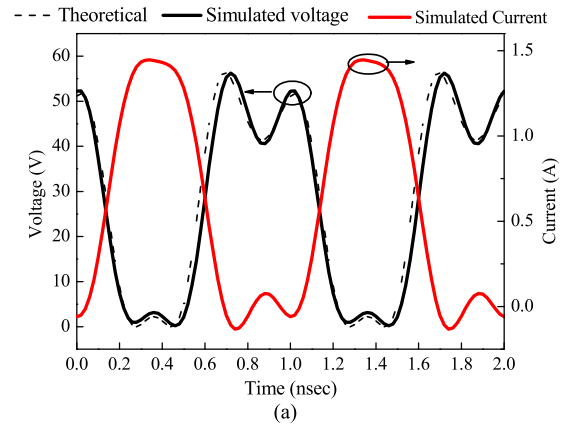In circuit design, the targeted frequency band from 0.5 GHz to 3.15 GHz is divided into four frequency sections (0.5–1 GHz, 1-1.5 GHz, 1.5-2.4 GHz, and 2.4-3.15 GHz). The load impedances at 0.7, 1.2, 1.9 and 2.8 GHz are chosen to represent the optimal impedance of the four frequency sections. The design procedures are summarized as follows:

Firstly, the optimal impedances at the four selected frequency points are extracted by using load-pull simulation in ADS. The extracted impedances at the intrinsic-drain plane and the corresponding impedances at the package plane are

$$Z_{in} = Z_{L3} \frac{Z_L(Z_{L4} - Z_{L3}\tan(\theta_{L3})\tan(\theta_{L4})) + jZ_{L4}(Z_{L4}\tan(\theta_{L4}) + Z_{L3}\tan(\theta_{L3})\tan(\theta_{L4}))}{Z_{L4}(Z_{L3} - Z_{L4}\tan(\theta_{L3})\tan(\theta_{L4})) + jZ_L(Z_{L3}\tan(\theta_{L4}) + Z_{L4}\tan(\theta_{L3}))} \quad (8)$$
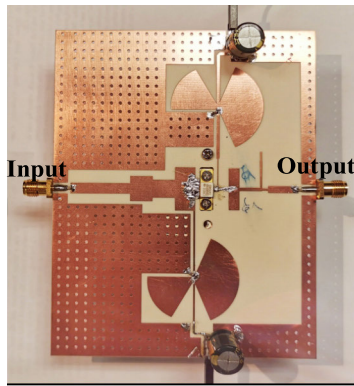
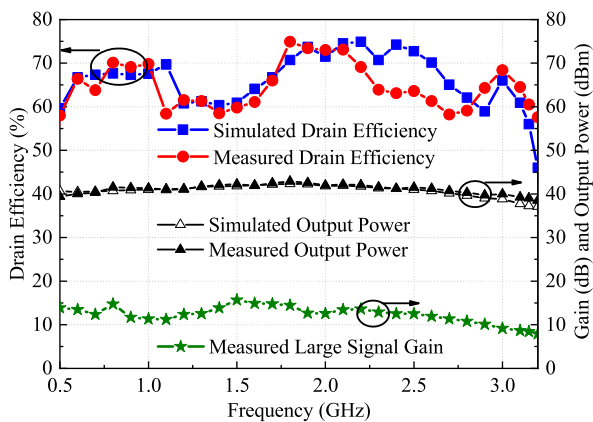**FIGURE 12.** Photograph of the fabricated broadband PA.

FIGURE 13. Simulated and measured drain efficiency, output power and large signal gain over the entire operation bandwidth.

FIGURE 14. Simulated and measured output power (P_{out}) versus frequency.
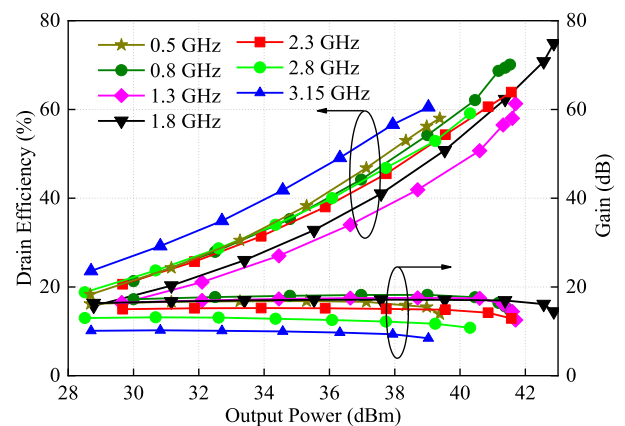
FIGURE 15. Measured gain and drain efficiency against output power at different frequencies.

TABLE 1. Dimensions of the proposed broadband PA.

TL	T1	T2	T3	T4	T5	T6	T7	T8	T9	T10
W (mm)	1.77	3.7	8.82	6.3	15.1	0.6	7.1	1.4	0.4	1
L (mm)	5	19.8	7.5	7.4	6.7	22	1.6	1.6	9.5	16.5
TL	T11	T12	T13	T14	T15	T16	T17	T18	T19	T20
W (mm)	1	3.5	3.5	1.2	0.55	0.75	0.55	0.8	2.4	1.77
L (mm)	3.4	7.3	7.3	8	2.9	6.5	3	2	10	5

plotted in Fig. 8(a). Based on (3) and (4), the solutions for the fundamental and harmonic frequencies can be calculated by varying γ from -0.1 to 0.6, δ from 0.4 to 0.6 and ζ from -1 to 1, which are illustrated in Fig. 8(b). From Figs. 8 (a) and (b), the simulated optimum impedances at intrinsic-drain plane are approximate to those derived from theory in Section II-A. Thus, the simulated optimum impedances at package plane can meet the requirements of the proposed combination of CCF and CCF^{-1} PA modes, which can be used to calculate the design parameters of the proposed LP OMN.

Secondly, based on the theoretical analysis on Sections II-B and C, the initial parameters of proposed LP OMN can be determined.

Thirdly, a wideband input matching network is designed by using multiple stepped-impedance transmission line sections to cover the whole operation bandwidth.

Finally, fine-tuning of the whole circuit with the equivalent nonlinear large-signal model in Fig. 7 is performed to obtain high efficiency over the whole operation bandwidth.

Based on the above design procedures, a broadband PA is proposed with the schematic shown in Fig. 9. Simulated impedances at the package plane (Z_{OMN}) and the intrinsic-drain plane ($Z_{OMN,D}$) are shown in Figs. 10(a) and (b), respectively. It can be seen that the proposed LP OMN
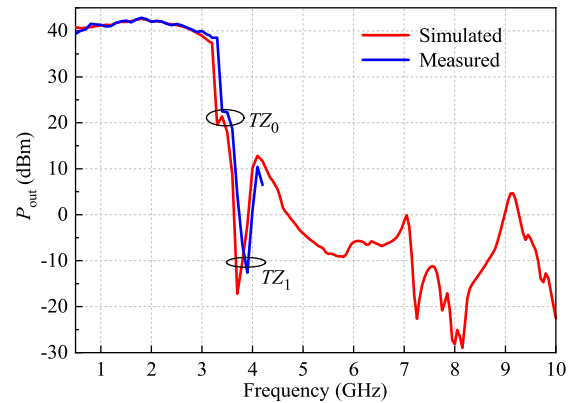
can achieve a wideband matching within the whole operation bandwidth from 0.5 GHz to 3.15 GHz. The simulated fundamental impedances are slightly different from the initial targeted load impedances, which are acceptable for high efficiency. The second harmonic impedances locate within or near the targeted design space. The design parameters of the proposed broadband PA are tabulated in Table 1.

B. WAVEFORM ENGINEERING

Figs. 11(a), (b) and (c) show the theoretical and simulated time-domain intrinsic-drain voltage and current waveforms

FIGURE 16. Measured spectra using a 20-MHz LTE signal with and without DPD (a) at 0.5 GHz; (b) at 0.9 GHz; (c) at 1.3 GHz; (d) at 1.3 GHz; (e) at 1.8 GHz; (e) at 2.6 GHz; (f) at 3.1 GHz.
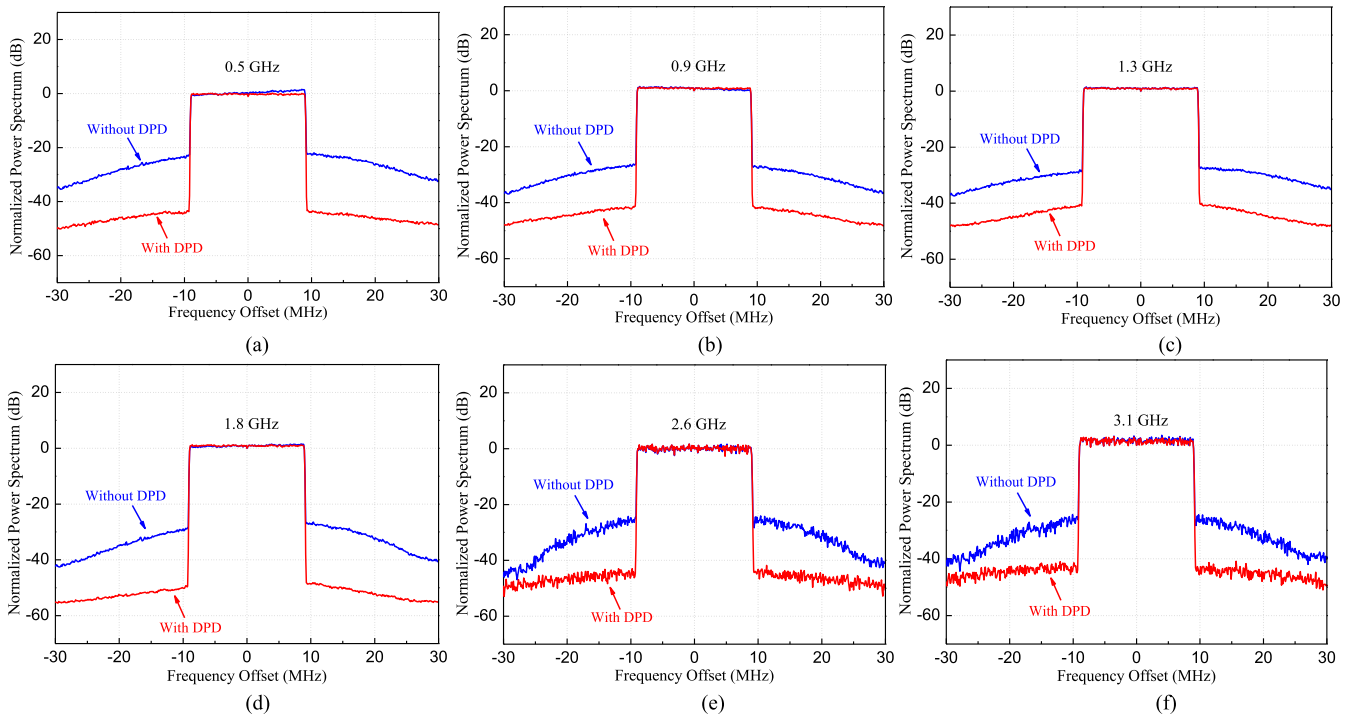
under saturated output power operating at 1 GHz, 2 GHz, and 3 GHz, respectively. In Fig. 11(a), the waveform at 1 GHz agrees well with that of the extended CCF PA mode when $\gamma = -0.05$ and $\delta = 0.47$. The quasi CCF^{-1} waveforms at 2 GHz and 3 GHz can be observed in Figs. 11(b) and (c), respectively, when the design factors are chosen as $\zeta = 0.22$ and $\zeta = -0.3$.

IV. EXPERIMENT

A. CONTINUOUS-WAVE (CW) MEASUREMENTS

For demonstration, the proposed broadband PA is fabricated. The photograph of the fabricated circuit is shown in Fig. 12. The large-signal responses are measured by the Agilent EXG Vector Signal Generator N51728 and Agilent EXA Signal Analyzer N9010A.

Fig. 13 shows the simulated and measured drain efficiency, output power and gain over the entire operation bandwidth under continuous-wave (CW) excitation. Good agreement between the simulated and measured results can be observed. Within the operation bandwidth from 0.5 to 3.15 GHz (an FBW of 145.2%), the drain efficiency is measured as 58%-74.9%. The measured large-signal gain ranges from 8.43 dB to 15.67 dB. With the gain compression of around 3 dB, the saturation output power is measured from 39.03 dBm to 42.87 dBm. Fig. 14 shows the simulated and measured output powers versus frequency which realize wide operation passband. Two TZs (TZ_0 and TZ_1) are generated at the passband edge, resulting in a sharp roll-off rate from the passband to stopband. Since we do not have a drive amplifier that can work in such a wide bandwidth from 0.5 to 10GHz,

TABLE 2. Comparison with some broadband PAs.

Ref.	Operation band (GHz)	FBW (%)	Drain efficiency (%)	P_{out} (dBm)	Gain (dB)
[8]	1.35-2.5	60	68-82	41.1-42.5	15.2-17
[9]	0.8-3.2	120	57-74	39.7-42.9	10.7-14.1
[10]	1.15-2.2	63	70-83	40.5-43.2	11.3-13.7
[11]	1.3-3.3	87	60-83	40-40.4	10-13
[13]	0.5-2.3	128.5	60-81	39.2-41.2	11.7-25.3
This work	0.5-3.15	145.2	58-74.9	39.03-42.87	8.43-15.67

the large-signal output power above 4.2 GHz is not measured. However, from the simulated result, it can be known that the proposed LP OMN achieves a wide stop-band with a high rejection of up to 10 GHz (higher than 3 f_{H2}).

Fig. 15 shows the measured drain efficiency and gain versus output power at different frequencies. It can be seen that a highest drain efficiency of 74.9% is measured at 1.8 GHz with an output power of 42.87 dBm and a gain of 15.67 dB. The measured lowest output power is 39.03 dBm at 3.15 GHz with a drain efficiency of 60.4% and a gain of 8.43 dB. The gain variation within the passband from 0.5 to 2.8 GHz is small whereas that from 2.8 to 3.15 GHz is a bit large. It is because the insert loss at the passband edge of around 3.15 GHz is relatively higher.

Table 2 shows the comparison with some reported broadband PAs using the same transistor. The proposed PA shows

TABLE 3. Linearity performance for 20-MHz LTE signal.

Frequency (GHz)	ACLR (dBc)		Output Power (dBm)
	Without DPD	With DPD	
0.5	-27.95/-26.09	-45.82/45.64	33.95
0.9	-30.70/-31.08	-45.06/45.38	35.01
1.3	-32.51/-30.55	-45.65/-45.33	35.73
1.8	-34.74/32.07	-53.75/-52.87	33.95
2.6	-30.89/-29.78	-46.16/46.20	34.82
3.1	-32.90/-32.61	-45.78/-46.62	32.45

a wide operational bandwidth attribute to the combination of CCF^{-1} and extended CCF modes. The performance in terms of the gain, output power, and drain efficiency is comparable to those in [8]–[11], [13]. These demonstrate that the proposed quasi-elliptic low-pass matching network is effective in designing a broadband high-efficiency PA.

B. LTE MODULATED-SIGNAL MEASUREMENTS
To evaluate the linearity of the proposed PA, a 20-MHz long-term-evolution (LTE) signal with a peak-to-average power ration (PAPR) of 7.5 dB is used in this measurement. The LTE signal is generated by a vector signal generator (R&S SMW200A), and then amplified by a linear driver with sufficient driving power, and finally used to excite the proposed broadband PA. The measurement is accomplished using Spectrum analyzer R&S FSW43.

In order to verify that the fabricated PA has the potential to linearly amplify the modulated signal, DPD technique is undertaken. The measured spectrums with and without DPD are shown in Fig. 16. The lower and upper ACLRs of the broadband PA without DPD at ±20 MHz offset are measured from −26.09 dBc to −32.9 dBc, while those with DPD are measured better than −45.06 dBc with the output power of 32.45-35.95 dBm, showing improved linearity. The detailed measured results are summarized in Table 3.

V. CONCLUSION
We have proposed a quasi-elliptic low-pass output matching network for designing a broadband PA. The CCF^{-1} and extended CCF PA modes have been combined to significantly expand the design space for achieving a wide operation bandwidth. Analysis of the design parameters of the proposed quasi-elliptic low-pass output matching network has been detailed. For verification, the proposed PA has been fabricated and measured, showing high drain efficiency of 58%-74.9% within a wide operation bandwidth from 0.5 GHz to 3.15 GHz. A wide stopband from 3.4 GHz to 10 GHz and a sharp roll-off rate from the passband to stopband have been achieved. When measured with a 20-MHz LTE signal combined with the DPD technique, the proposed PA has shown good linearity with the ACLR below −45.06 dBc.

REFERENCES
[1] S. Y. Zheng, Z. W. Liu, Y. M. Pan, Y. Wu, W. S. Chan, and Y. Liu, "Bandpass filtering Doherty power amplifier with enhanced efficiency and wideband harmonic suppression," *IEEE Trans. Circuits Syst. I, Reg. Papers*, vol. 63, no. 3, pp. 337–346, Mar. 2016.
[2] B. Zhang, Y. Liu, C. Yu, Y. Wu, and G. Dong, "Filtering push-pull power amplifier based on novel impedance transformers," *Electron. Lett.*, vol. 52, no. 17, pp. 1467–1469, Aug. 2016.
[3] L. Gao, X. Y. Zhang, S. Chen, and Q. Xue, "Compact power amplifier with bandpass response and high efficiency," *IEEE Microw. Wireless Compon. Lett.*, vol. 24, no. 10, pp. 707–709, Oct. 2014.
[4] J.-X. Xu and X. Y. Zhang, "Dual-channel dielectric resonator filter and its application to Doherty power amplifier for 5G massive MIMO system," *IEEE Trans. Microw. Theory Techn.*, vol. 66, no. 7, pp. 3297–3305, Jul. 2018.
[5] Z. Wang, S. Gao, F. Nasri, and C.-W. Park, "High power added efficiency power amplifier with harmonic controlled by UWB filter with notched band at 6.42 GHz," in *Proc. WAMICON Conf.*, Apr. 2011, pp. 1–4.
[6] K. Chen and D. Peroulis, "A 3.1-GHz class-F power amplifier with 82% power-added-efficiency," *IEEE Microw. Wireless Compon. Lett.*, vol. 23, no. 8, pp. 436–438, Aug. 2013.
[7] S. Chen and Q. Xue, "A class-F power amplifier with CMRC," *IEEE Microw. Wireless Compon. Lett.*, vol. 21, no. 1, pp. 31–33, Jan. 2011.
[8] M. Yang, J. Xia, Y. Guo, and A. Zhu, "Highly efficient broadband continuous inverse class-F power amplifier design using modified elliptic low-pass filtering matching network," *IEEE Trans. Microw. Theory Techn.*, vol. 64, no. 5, pp. 1515–1525, May 2016.
[9] J. Wang, S. He, F. You, W. Shi, J. Peng, and C. Li, "Codesign of high-efficiency power amplifier and ring-resonator filter based on a series of continuous modes and even–odd-mode analysis," *IEEE Trans. Microw. Theory Techn.*, vol. 66, no. 6, pp. 2867–2878, Jun. 2018.
[10] Z. Yang, Y. Yao, Z. Liu, M. Li, T. Li, and Z. Dai, "Design of high efficiency broadband continuous class-F power amplifier using real frequency technique with finite transmission zero," *IEEE Access*, vol. 6, pp. 61983–61993, 2018.
[11] K. Chen and D. Peroulis, "Design of broadband highly efficient harmonic-tuned power amplifier using in-band continuous class-F$_{-1}$/F mode transferring," *IEEE Trans. Microw. Theory Techn.*, vol. 60, no. 12, pp. 4107–4116, Dec. 2012.
[12] Z. Lu and W. Chen, "Resistive second-harmonic impedance continuous Class-F power amplifier with over one octave bandwidth for cognitive radios," *IEEE J. Emerg. Sel. Topics Circuits Syst.*, vol. 3, no. 4, pp. 489–497, Dec. 2013.
[13] S. Y. Zheng, "Design of ultrawideband high-efficiency extended continuous class-F power amplifier," *IEEE Trans. Ind. Electron.*, vol. 65, no. 6, pp. 4661–4669, Jun. 2018.
[14] V. Carubba, A. L. Clarke, M. Akmal, J. Lees, J. Benedikt, S. C. Cripps, and P. J. Tasker, "The continuous inverse-F mode power amplifier with resistive second harmonic impedance," *IEEE Trans. Microw. Theory Techn.*, vol. 60, no. 6, pp. 1928–1936, Jun. 2012.
[15] Z. Zhuang, Y. Wu, Q. Yang, M. Kong, and W. Wang, "Broadband power amplifier based on a generalized step-impedance quasi-chebyshev lowpass matching approach," *IEEE Trans. Plasma Sci.*, vol. 48, no. 1, pp. 311–318, Jan. 2020.
[16] L. Zhu, S. Sun, and R. Li, *Microwave Bandpass Filters for Wideband Communications*. New York, NY, USA: Wiley, 2012.
[17] Y. Zhuang, Z. Fei, A. Chen, Y. Huang, K. Rabbi, and J. Zhou, "Design of multioctave high-efficiency power amplifiers using stochastic reduced order models," *IEEE Trans. Microw. Theory Techn.*, vol. 66, no. 2, pp. 1015–1023, Feb. 2018.
[18] P. Tasker and J. Benedikt, "Waveform inspired models and the harmonic balance emulator," *IEEE Microw. Mag.*, vol. 12, no. 2, pp. 38–54, Apr. 2011.

HANG CHEN was born in Fuzhou, Fujian, China. He received the B.S. degree in electronic and information engineering from the Taiyuan University of Technology, Taiyuan, China, in 2016. He is currently pursuing the Ph.D. degree with the School of South China University of Technology, Guangzhou, China. His current research interests include broadband high-efficiency power amplifier theory and design techniques.

IEEE *Access*

H. Chen *et al.*: Broadband High-Efficiency Power Amplifier With Quasi-Elliptic Low-Pass Response

JIN-XU XU was born in Meizhou, Guangdong, China. He received the B.S. degree in electronic engineering from the South China University of Technology, Guangzhou, China, in 2015. He is currently pursuing the joint Ph.D. degree with the School of Electronic and Information Engineering, South China University of Technology, and the School of Electrical Data Engineering, University of Technology Sydney, Ultimo, NSW, Australia.

From 2014 to 2015, he was a Research Assistant with the Shenzhen Key Laboratory of Millimeter-Wave and Wideband Wireless Communications (MWWC), CityU Shenzhen Research Institute, Shenzhen, China. He has authored or coauthored more than 40 internationally refereed journals/conference papers. He is the co-inventor of nine granted Chinese patents and two granted U.S. patents. His current research interests include microwave and terahertz circuits.

Mr. Xu was a recipient of the Best Student Paper Award presented at the IEEE MTT-S International Microwave Workshop Series on Advanced Materials and Processes for RF and THz Applications (IMWS-AMP), Chengdu, China, in 2016. He is a Reviewer of several internationally refereed journals, including the IEEE Transactions on Industrial Electronics and the IEEE Transactions on Microwave Theory and Techniques.

WEN-HUA CHEN (Senior Member, IEEE) received the B.S. degree in microwave engineering from the University of Electronic Science and Technology of China (UESTC), Chengdu, in 2001, and the Ph.D. degree in electronic engineering from Tsinghua University, Beijing, China, in 2006.

From 2010 to 2011, he was a Postdoctoral Fellow with the Intelligent RF Radio Laboratory (iRadio Lab), University of Calgary. He is currently a Professor with the Department of Electronic Engineering, Tsinghua University. He has authored or coauthored more than 120 journals and conference papers. His main research interests include power-efficiency enhancement for wireless transmitters, PA predistortion, and smart antennas.

Dr. Chen was a recipient of the 2015 Outstanding Youth Science Foundation of NSFC, the 2014 URSI Young Scientist Award, and the Student Paper Awards of several international conferences. He is an Associate Editor of the *International Journal of Microwave and Wireless Technology* and also an Associate Editor of the IEEE Transactions on Microwave Theory and Techniques.

XIU YIN ZHANG (Senior Member, IEEE) received the B.S. degree in communication engineering from the Chongqing University of Posts and Telecommunications, Chongqing, China, in 2001, the M.S. degree in electronic engineering from the South China University of Technology, Guangzhou, China, in 2006, and the Ph.D. degree in electronic engineering from the City University of Hong Kong, Hong Kong, in 2009.

From 2001 to 2003, he was with ZTE Corporation, Shenzhen, China. He was a Research Assistant from July 2006 to June 2007 and a Research Fellow from September 2009 to February 2010 with the City University of Hong Kong. He is currently a Full Professor and the Vice Dean of the School of Electronic and Information Engineering, South China University of Technology. He also serves as the Vice Director of the Guangdong Key Laboratory of Millimeter-Wave and Terahertz and the Vice Director of the Engineering Research Center for Short-Distance Wireless Communications and Network, Ministry of Education. He has authored or coauthored more than 140 internationally refereed journal articles (including more than 80 IEEE Transactions) and around 80 conference papers. His research interests include antennas and arrays, MMIC, microwave/terahertz circuits and sub-systems, and wireless communications.

Dr. Zhang is a Fellow of the Institution of Engineering and Technology. He has served as a General Chair/Technical Program Committee (TPC) Chair/ Member, and a Session Organizer/Chair for a number of conferences. He was a recipient of the National Science Foundation for Distinguished Young Scholars of China, the Leading Talent of Technological Innovation of Ten-Thousands Talents Program, and the Young Scholar of the Changjiang Scholars Program of Chinese Ministry of Education. He was a recipient of the Scientific and Technological Award (First Honor) of Guangdong Province. He was the Supervisor of several conference best paper award winners.

ZHI-HUA KONG was born in Xianning, Hubei, China. He received the B.S. degree in communication engineering from the Wuhan University of Technology, Wuhan, China, in 2017. He is currently pursuing the M.S. degree with the School of Information and Communication Systems, South China University of Technology, Guangzhou, China. He is currently involved in high-efficiency RF broadband amplifier design and digital transmitter.

• • •

52574

VOLUME 8, 2020